# Fiber Bragg grating tether used to measure drag forces in neutral buoyancy flow tank tests

S. A. Wade, W. Jolley, and A. Fouras
*Department of Mechanical Engineering, Monash University, Clayton, Victoria 3800, Australia*

(Received 6 February 2008; accepted 5 May 2008; published online 3 June 2008)

The drag exerted on neutrally buoyant tethered spheres in a flow tank was measured as a function of flow rate. A unique solution to the problem was achieved using an optical fiber including a Bragg grating sensor as part of the tether. Measurements of the strain on the tether taken at flow rates between 0.14 and 0.33 m/s, were used to determine drag forces for spheres with diameters ranging from 40 to 100 mm. Vortex-induced vibration was observed in tests performed at Reynolds numbers from $5\times10^3$ to $4.5\times10^4$. The drag coefficients for these tests were found to range from 0.51 to 0.77. © *2008 American Institute of Physics.* [DOI: 10.1063/1.2937457]

## I. INTRODUCTION

Tethered spherical structures are used in a wide range of applications such as marine buoys, underwater mines, and tethered balloons in the atmosphere. When placed in a flowing fluid, such as moving water or air, a spherical structure will be subject to a drag force and, in some cases, the interaction between the sphere and the fluid will result in vortices to be formed that cause the sphere to vibrate. As such, there is interest to determine how tethered spherical structures move in a flowing fluid. Investigations of this nature are typically carried out using water or wind tunnels, with the position of the sphere with time typically monitored using either video cameras or displacement transducers.[1–4]

There have been a large number of experimental and theoretical investigations carried out on the fluid dynamic drag of spheres (for example, see Refs. 5–8 and references therein). The drag force $F_d$ on a sphere is given by (e.g., Ref. 8)

$$F_d = \frac{1}{2}C_d\rho U^2\frac{1}{4}\pi D^2, \tag{1}$$

where $C_d$ is the drag coefficient, $\rho$ is the fluid density, $U$ is the free stream velocity, and $D$ is the diameter of the sphere. In fluid dynamics, the dimensionless Reynolds number Re is used to assist in defining the flow regime for an object,[9] which is given by

$$\mathrm{Re} = \frac{\rho U D}{\mu}, \tag{2}$$

where $\mu$ is the viscosity of the fluid. In this work, measurements have been made for Reynolds numbers ranging from $\sim5\times10^3$ to $\sim4.5\times10^4$. For the case of a stationary sphere, the drag coefficient has commonly been reported as relatively constant over this range of Reynolds numbers at $\sim0.4$.[5–9] Recent data for the case of a tethered sphere, however, have indicated that vibration of the sphere may increase the drag coefficient significantly.[1,2] The drag, in these recent reports, has been estimated using the mean angle of inclination of the sphere.

In the current work, we discuss the use of an optical fiber Bragg grating incorporated in the tether used to hold the sphere, to provide a direct measurement of the force exerted onto the sphere by a moving fluid. Fiber Bragg gratings were first discovered in the 1970s and have since been utilized in both telecommunications and sensing applications.[10,11] They are now a mature sensing technology, used to measure a wide range of parameters, and commercial sensors and interrogation systems are readily available. Some of the advantages of fiber Bragg grating sensors are their small size and weight, their immunity to electromagnetic interference, and the possibility of multiplexing many sensors together on a single optical fiber.

Optical fiber Bragg gratings are typically manufactured by exposing an optical fiber to spatially modulated high intensity UV radiation that results in periodic changes in the refractive index of the core of the fiber. The refractive index pattern written into the fiber core acts as a wavelength specific light reflector. For a standard Bragg grating type, the center wavelength of the reflected light $\lambda_{\mathrm{Bragg}}$ is proportional to the effective refractive index of the grating $n$ and the spacing between adjacent changes in the refractive index, known as the grating pitch $\Lambda$;

$$\lambda_{\mathrm{Bragg}} = 2n\Lambda. \tag{3}$$

Sensors based on fiber Bragg gratings typically use the change in the wavelength of the grating caused by changes in the grating pitch or effective refractive index to measure the parameter of interest. Applying strain to the fiber, for example, increases the grating pitch and also changes the refractive index due to the photoelastic effect.

Fiber Bragg grating sensors have found widespread use in the field of civil engineering where they are used to monitor the health of large structures, such as bridges, dams, and offshore oil rigs. Despite their potential advantages, fiber Bragg gratings have, however, found limited application in the discipline of fluid dynamics. Jin *et al.*[12] used a fiber Bragg grating to monitor the flow-induced vibration of a circular cylinder in a wind tunnel by attaching the grating to the cylinder and distributed flow measurements have been demonstrated using Bragg gratings in a manner analogous to heated wire anemometry by Willish *et al.*[13] In other related work, it is also important to mention the study by Edwards

 © 2008 American Institute of Physics

Downloaded 02 Aug 2011 to 136.186.80.71. Redistribution subject to AIP license or copyright; see http://rsi.aip.org/about/rights_and_permissions

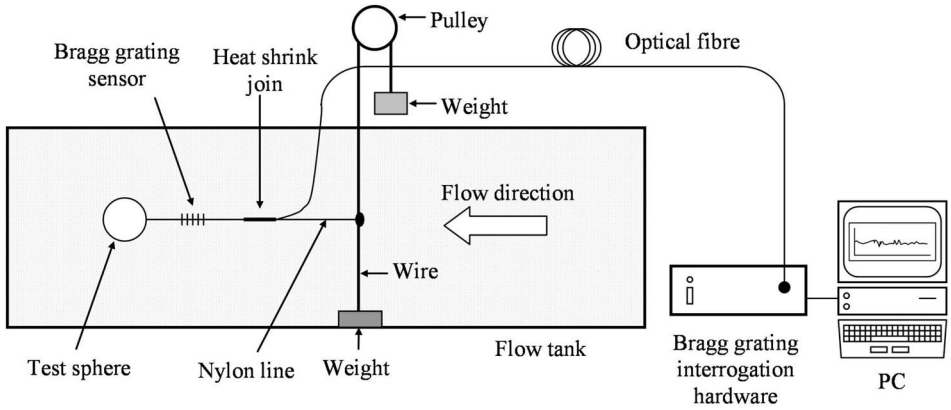


FIG. 1. Flow tank arrangement used to test the drag force on neutrally buoyant spheres.

who used Fabry–Pérot-based optical fiber sensors on a sting balance to investigate the aerodynamic properties of a model in a supersonic wind tunnel.[14]

As mentioned above, we have measured the drag on spheres in a flow tank using optical fiber Bragg grating sensors. For this case, the drag force on a sphere $F_{\text{drag}}$ is related to strain measured by the Bragg grating $\varepsilon$ via

$$F_{\text{drag}} = E\varepsilon A, \tag{4}$$

where $E$ and $A$ are the Youngs modulus and cross-sectional area of the sensor. The sensing arrangement is unique in that the small dimensions of the sensor allow measurements to be made with minimal disruption to the flow upstream to the sphere. In addition, the use of an optical-based sensor removes some of the potential dangers involved when using electrical sensors submerged in water. In this work, tests have been carried out using neutrally buoyant spheres so that drag rather than buoyancy is the parameter measured.

## II. EXPERIMENTAL DESIGN

Tests were undertaken to measure the drag on a number of neutrally buoyant spheres, using a fiber Bragg grating sensor, in a fluid flow tank. Details of the test arrangements used are provided below.

### A. Flow tank

The experiments were carried out in a free surface water channel, with a 600 mm width, 800 mm depth, and 4000 mm length. The speed range used was between 0.14 and 0.46 m/s. The turbulence intensity level of this channel has been measured to be less than 1%.

Figure 1 shows the general test arrangement used in this work. To hold the sphere in place during testing, the instrumented fiber optic tether attached to the sphere was joined to a piece of nylon line which was, in turn, tied to a vertical tether. In an initial proof of principal test, the vertical tether consisted of a piece of string that was fixed between a weight on the bottom of the flow tank and a fixture directly above the flow tank. During the initial tests, it was noticed that the vertical string tended to vibrate when the flow rates approached the maximum rates tested. To help minimize these vibrations, a new design was implemented with a pulley system used to create a tension of ~150 N in the vertical wire to which the tether was attached. This tension was designed, assuming a drag coefficient of 0.4, to allow a maximum deflection in the direction of the flow of approximately 0.5 mm for the case of a 100 mm diameter sphere at a 0.46 m/s flow velocity. The temperature of the water in the flow tank was monitored during tests using a Fluke 53II thermometer.

### B. Sphere design

Initially, a proof of principal test was carried out using a table tennis ball filled with water as the test sphere. The design of the sphere and tether sensor for this case is shown in Fig. 2. The optical fiber tether containing the Bragg grating was approximately 260 mm in length with the grating located close to the middle of the tether. The density of the material used in the table tennis ball, and the materials used to attach the tether, caused this sphere design to sink slowly when placed in the flow tank. However, it was believed that buoyancy effects would be relatively small compared to drag, especially at higher flow speeds, and therefore, the design to be more than adequate for the purposes of this initial test.

To reduce buoyancy effects on the measurements and also to increase the range of drag measurements, additional

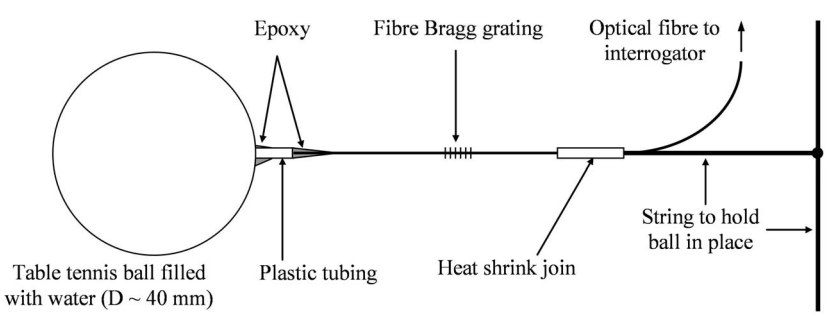


FIG. 2. Detail of the initial sensing and tether arrangement (Note: not to scale).

Downloaded 02 Aug 2011 to 136.186.80.71. Redistribution subject to AIP license or copyright; see http://rsi.aip.org/about/rights_and_permissions

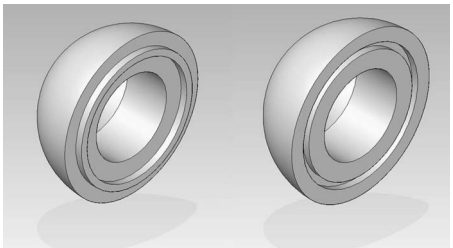

FIG. 3. Modified design of neutrally buoyant spheres, showing the two-halves which connect together.

spheres of a new design were manufactured. After taking into consideration the issues of density and ease of manufacture, the new spheres were made using Perspex. As shown in Fig. 3, the new spheres were manufactured as two-halves which snap fit together. The spheres were hollowed out to achieve neutral buoyancy, with a small additional amount of material removed to allow for fine adjustments to be made. Two spheres of this design were manufactured with outer diameters of 70 and 100 mm. Optical fiber tethers were joined to the new sphere designs using a small section of plastic tubing for strain relief in a similar manner to the initial design. A tether length of ~1.0 m in total was used for the data reported for the later sphere design. The 70 mm diameter sphere was found to have very good neutral buoyancy, while the 100 mm diameter sphere was found to sink although very slowly.

### C. Fiber Bragg gratings

The fiber Bragg gratings used in this work were written in standard single-mode telecommunications-type optical fiber using a phase mask method. Prior to writing the gratings, the fiber was sensitised via high pressure hydrogen loading. To prevent drift in the Bragg gratings due to hydrogen outgassing, the gratings were subjected to an annealing process at 330 °C for 2.5 min shortly after manufacture. Details of the relevant properties of the Bragg gratings are given in Table I.

Changes in the reflected center wavelength of the Bragg gratings were monitored during the tests using a Micron Optics fiber Bragg grating interrogation system, with measurements made at 52 Hz. While the model of interrogation system used in this work has since been superseded by designs with increased accuracy, it was believed that it was more than adequate for the tests undertaken. A calibration factor, ~1.2 $\mu\varepsilon$/nm, determined prior to the tests was used to convert wavelength changes to changes in strain.

TABLE I. Properties of the fiber Bragg gratings used in this work, $L$: grating length, $\lambda$: center wavelength, $R$: reflectance, and FWHM: full width at half maximum grating bandwidth.

| Sphere Diameter (mm) | Fiber Bragg grating properties | | | |
|---|---|---|---|---|
| | $L$ (mm) | $\lambda$ (nm) | $R$ (dB) | FWHM (nm) |
| 40 | 4 | 1546 | −19.5 | 0.17 |
| 70 | 4 | 1546 | −55.1 | 0.44 |
| 100 | 4 | 1545 | −39.3 | 0.21 |

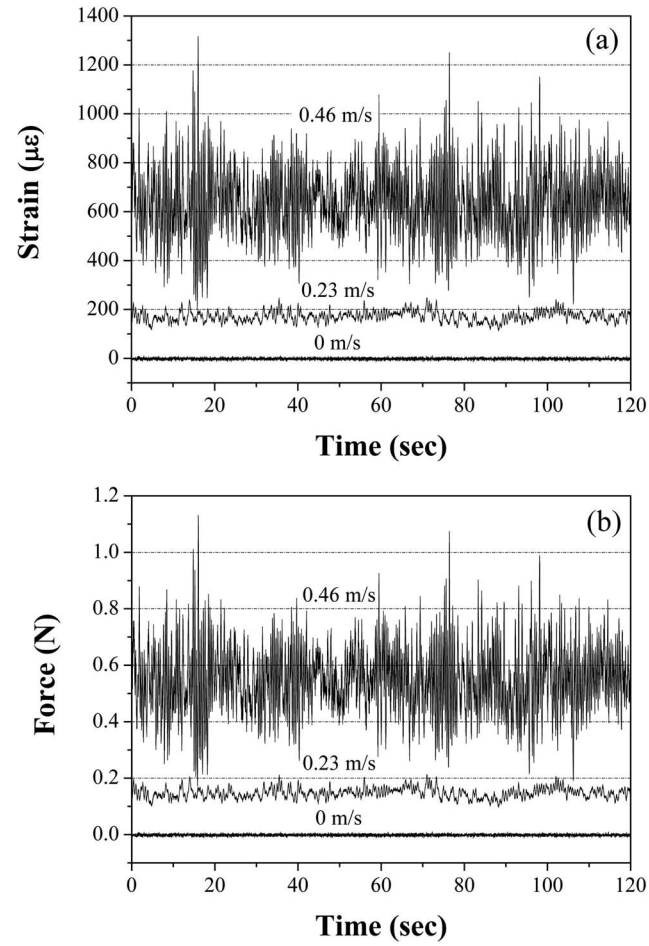


FIG. 4. (a) Strain and (b) drag force on 100 mm diameter sphere in flow tank vs time at various flow rates (tether length of 1 m).

## III. RESULTS

The strain on the tether due to drag on the spheres was measured for a number flow rates between 0.14 and 0.33 m/s for the initial test and 0.14 and 0.46 m/s for the tests with the two larger spheres. These values allowed a range of Reynolds numbers between $\sim 5\times 10^3$ and $\sim 4.5\times 10^4$ to be investigated. At each particular flow rate, Bragg grating readings were taken after allowing the flow to stabilize for a period of 5–10 min to ensure stable conditions with low turbulence intensity. Typically, 1–2 min of fiber Bragg grating data was recorded at each flow rate.

Examples of the strain for the 100 mm diameter sphere measured by the Bragg grating sensor and the corresponding drag force, calculated using Eq. (4), are shown in Fig. 4. During the tests, it was observed that, at increased flow rates, the spheres tended to start pulsing back and forth in the direction of the fluid flow, the amplitude of which increased with flow rate. As such, the noise in the measured signal appears to increase with flow rate. This behavior has been observed previously[1,2] and has been attributed to vortex-induced vibration. By plotting a limited time range of Fig. 4(a), the vibrations can clearly be seen (see Fig. 5).

The average strain, and corresponding average drag force, measured at each of the flow rates for each of the spheres are shown in Fig. 6. The error bars shown are the

Downloaded 02 Aug 2011 to 136.186.80.71. Redistribution subject to AIP license or copyright; see http://rsi.aip.org/about/rights_and_permissions

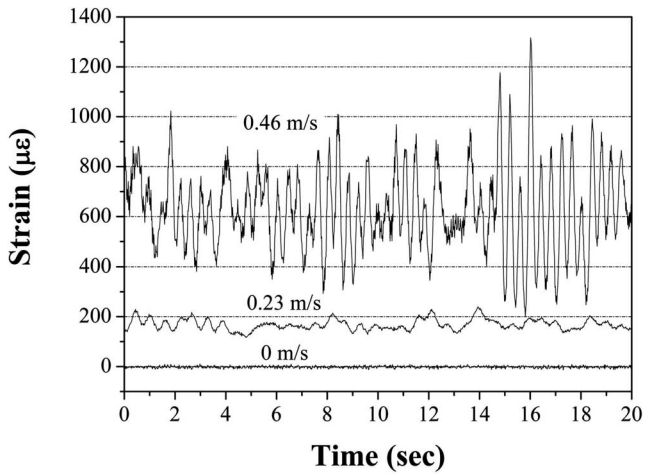


FIG. 5. As for Fig. 4(a) but with reduced time range to show vortex-induced vibrations at increased flow rates.

standard deviation of the measurement at each flow rate tested. Also shown in Fig. 6 are the theoretical strain and drag forces for the spheres calculated using Eq. (1), assuming a constant drag coefficient. In the early stages of data analysis, a drag coefficient of ~0.4 was used to fit the data for all of the spheres tested, however, relatively poor fits

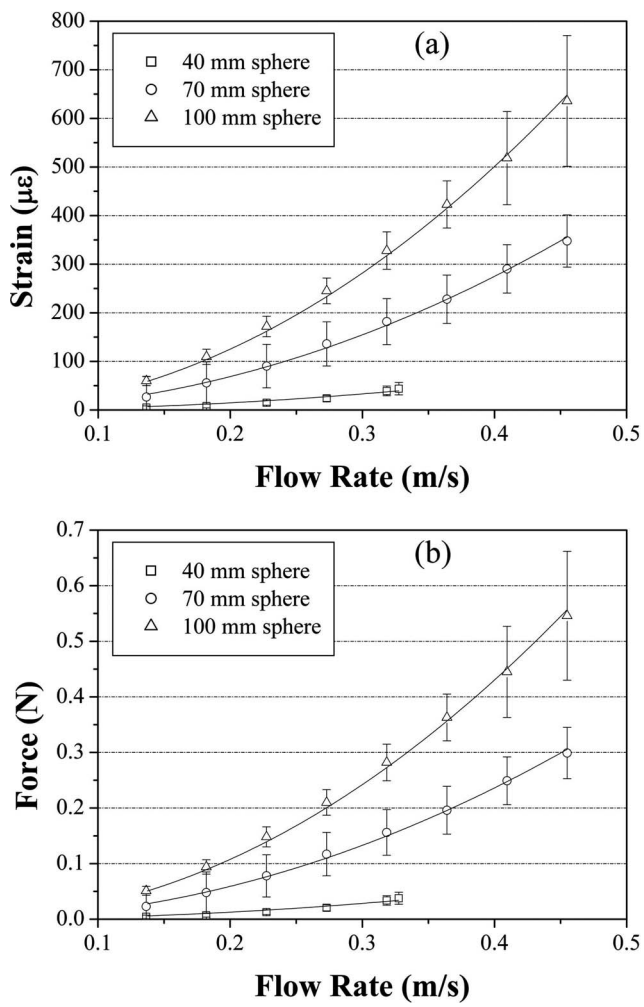


FIG. 6. (a) Strain and (b) drag force vs flow rate for the various spheres tested.

TABLE II. Results of drag coefficients obtained from fits to the force vs flow rate data assuming constant drag coefficient.

| Sphere diameter (mm) | Fit drag coefficient | $r^2$ |
|---|---|---|
| 40 | $0.51 \pm 0.03$ | 0.943 |
| 70 | $0.769 \pm 0.008$ | 0.998 |
| 100 | $0.686 \pm 0.006$ | 0.998 |

resulted. Subsequently, fits were made to the data with the drag coefficient as a free parameter, the results of which are given in Table II and were used in the plots shown in Fig. 6. Measurements of the fiber Bragg grating strain taken at the start and end of each test when the fluid was stationary, i.e., no flow, indicated that any drift in readings could be considered to be negligible.

Work by researchers at Cornell University[1,2] have shown that vibrations of a tethered sphere in a moving fluid result in a increase in the drag compared to the more commonly reported measurements of sphere drag, determined, for example, using a stationary sphere. The drag coefficient $C_d$ obtained in this work for the 100 mm diameter sphere is shown in Fig. 7 as a function of Reynolds number. Also shown in Fig. 7 for comparison are the data obtained by Williamson and Govardhan[2] for a tethered sphere, and a plot showing the more commonly reported sphere drag. The later plot was made using Eq. (19) from Ref. 8 in which a wide range of historical data was fitted.

## IV. DISCUSSION AND CONCLUSION

The present work has shown the use of an optical fiber Bragg grating sensor to measure the drag properties of neutrally buoyant tethered spheres in a flow tank. In an initial test to validate the sensing technique, several issues with the test arrangement were observed that were believed to be possible sources of measurement error, including vibration of the vertical tether used to hold the sphere and the buoyancy of the sphere. Changes to the test setup were made, including a new vertical tether arrangement and new sphere design. In subsequent testing, using the modified equipment, similar vi-

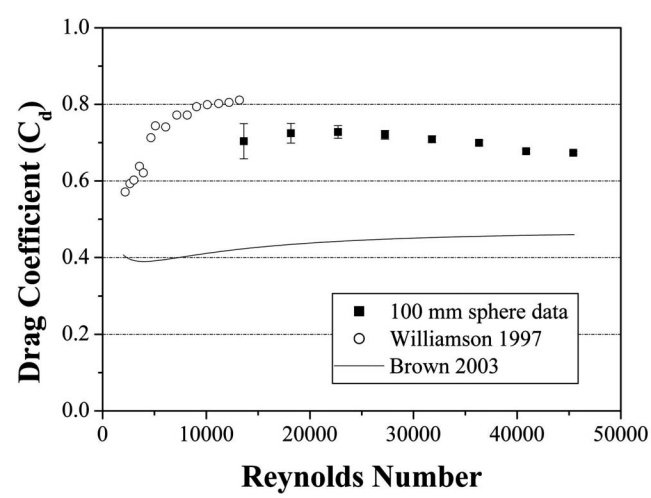


FIG. 7. Comparison of the sphere drag coefficient data obtained for the 100 mm sphere in this work with the values obtained by others.

Downloaded 02 Aug 2011 to 136.186.80.71. Redistribution subject to AIP license or copyright; see http://rsi.aip.org/about/rights_and_permissions

TABLE III. Standard deviation of fiber Bragg grating measurements obtained at 0 m/s flow for the various spheres tested, and signal-to-noise ratios for a flow rate of 0.32 m/s.

| Sphere diameter (mm) | Standard deviation | | SNR at 0.32 m/s |
|---|---|---|---|
| | Strain ($\mu\varepsilon$) | Force (N) | |
| 40 | 3.4 | $3.0\times10^{-3}$ | 11 |
| 70 | 40 | $3.5\times10^{-2}$ | 5 |
| 100 | 4.0 | $3.4\times10^{-3}$ | 82 |

brations to those observed in the initial test were found to occur. Indeed, oscillations of this type have been observed previously[1–4] and have been explained as being caused by vortex shedding. Calculations of the net force acting on the sphere used in the initial test, i.e., buoyancy minus weight, indicate a downward force of the order of 0.01 N. While this force is relatively small, at the slower flow rates tested with the initial sphere design, the additional vertical force will have caused an artificial increase in the drag forces calculated from the strain measurements. Improvements in the design of the spheres for the later measurements significantly reduced any forces in the vertical direction. As such, vertical forces are believed to have had negligible affect on the tests for the 70 and 100 mm spheres.

The strain measured by the fiber Bragg grating sensors was found to increase with increasing flow rate for each of the spheres tested as was expected. Indeed, excellent agreement was found between the measured change in the strain with flow rate and the theoretical change if the drag coefficient was used as a free fitting parameter. As has been seen previously, the drag coefficient for the case of a tethered sphere was measured to be significantly higher than the value of approximately 0.4 commonly reported for spheres for the range of Reynolds numbers investigated in this work. This increase in drag coefficient has been observed by previous researchers[1,2] and explained to be caused by vortex-induced vibrations, which were clearly observed during the tests undertaken.

With regards to the use of fiber Bragg gratings for this type of measurement, it is useful to discuss the measurement sensitivity. The noise in the Bragg grating sensors used for each of the spheres was obtained by taking measurements at the start and end of each test when the fluid was stationary, i.e., no flow. Typical standard deviations of these readings are given in Table III. Also shown are the forces that correspond to these strain values and the signal to noise ratios for a flow rate of 0.32 m/s. The noise for the fiber Bragg grating sensor used for the 70 mm diameter sphere was significantly larger than for the other two Bragg grating sensors. It is believed that the increased bandwidth of this Bragg grating may make it more difficult for the interrogator to identify the center wavelength of the grating resulting in a range of values possibly being recorded. The large bandwidth of this grating is related to its high reflectance. Initially, it was believed that the improved intensity of high reflectance Bragg gratings would reduce measurement noise; however, the results would indicate that the bandwidth of the Bragg reflectance may be a more important factor. There are a variety of ways to reduce the reflectance bandwidth of a Bragg grating including increasing the grating length and lowering the reflectance that may lead to reduced noise levels.

Another approach to improve the sensitivity of the fiber Bragg grating measurement is to use Bragg gratings with a smaller outer diameter. Using Eq. (4), it can be shown that reducing the diameter, and hence, cross-sectional area, of the Bragg grating results in increased changes in strain for the same applied force compared to a larger diameter fiber Bragg grating. Optical fiber Bragg gratings with reduced diameters can be achieved by either writing gratings in smaller diameter telecommunications-type optical fiber (e.g., diameter $=80\ \mu$m), available at relatively low cost, or by chemically etching the cladding. An order of magnitude improvement in sensitivity has been observed by previous researchers using a Bragg grating with a 40 $\mu$m diameter.[15] Improvements in sensor sensitivity are more critical for the smaller diameter spheres which have lower drag forces compared to larger diameter spheres at the same flow rate.

The use of an optical fiber Bragg grating sensor to measure the drag properties of neutrally buoyant spheres has been demonstrated. Excellent correlation has been found between the measured and theoretical drag forces as a function of flow rates. The drag coefficients of tethered spheres tested in this work, for Reynolds numbers between $\sim5\times10^3$ to $\sim4.5\times10^4$, were found to range from 0.51 to 0.77 which is significantly higher than the commonly reported value of $\sim$0.4 for spheres.

## ACKNOWLEDGMENTS

The authors would like to thank Paul Stoddart of Swinburne University for his assistance with fabricating the fiber Bragg gratings used in this work. The help of the staff in the Mechanical Engineering workshop at Monash University to manufacture the spheres and assist with the test rig was most appreciated.

[1] R. Govardhan and C. H. K. Williamson, J. Wind. Eng. Ind. Aerodyn. **69**, 375 (1997).
[2] C. H. K. Williamson and R. Govardhan, J. Fluids Struct. **11**, 293 (1997).
[3] N. Jauvtis, R. Govardhan, and C. H. K. Williamson, J. Fluids Struct. **15**, 555 (2001).
[4] R. N. Govardhan and C. H. K. Williamson, J. Fluid Mech. **531**, 11 (2005).
[5] F. W. Roos and W. W. Willmarth, AIAA J. **9**, 285 (1971).
[6] A. B. Bailey and J. Hiatt, AIAA J. **10**, 1436 (1972).
[7] H. Schlichting, *Boundary-Layer Theory*, 7th ed. (McGraw-Hill, New York, 1979), pp. 16–17.
[8] P. P. Brown and D. F. Lawler, J. Environ. Eng. **129**, 222 (2003).
[9] B. R. Munson, D. F. Young, and T. H. Okiishi, *Fundamentals of Fluid Mechanics*, 4th ed. (Wiley, New York, 2002).
[10] A. Othonos and K. Kyriacos, *Fiber Bragg Gratings: Fundamentals and Applications in Telecommunications and Sensing* (Artech House, Boston, 1999).
[11] A. D. Kersey, M. A. Davis, H. J. Patrick, M. LeBlanc, K. P. Koo, C. G. Askins, M. A. Putnam, and E. J. Friebele, J. Lightwave Technol. **15**, 1442 (1997).
[12] W. Jin, Y. Zhou, P. K. C. Chan, and H. G. Xu, Sens. Actuators, A **79**, 36 (2000).
[13] M. Willsch, T. Bosselmann, P. Kraemmer, and R. Gerner, *17th International Conference on Optical Fiber Sensors* (SPIE, Bruges, Belgium, 2005), Vol. 5855, pp. 286–289.
[14] A. T. Edwards, MS thesis, Virginia Tech, 2000.
[15] E. R. Lyons and H. P. Lee, IEEE Photonics Technol. Lett. **11**, 1626 (1999).

Downloaded 02 Aug 2011 to 136.186.80.71. Redistribution subject to AIP license or copyright; see http://rsi.aip.org/about/rights_and_permissions